Modeling and numerical results about the transverse argumental vibration of a beam excited axially by an harmonic motion transmitted through permanent or intermittent elastic contact (Working document).

Daniel Cintra, Gwendal Cumunel, Pierre Argoul

Transverse argumental vibration of a beam excited axially by an harmonic motion transmitted through permanent or intermittent elastic contact: modeling and numerical results

Daniel Cintra (corresponding author), Gwendal Cumunel
Université Paris-Est,
Laboratoire Navier (UMR 8205), CNRS, ENPC, IFSTTAR,
6 et 8, avenue Blaise Pascal,
Cité Descartes, Champs-sur-Marne,
F-77455 Marne La Vallée Cedex 2, France.
email: daniel.cintra@enpc.fr, gwendal.cumunel@enpc.fr
and
Pierre Argoul
IFSTTAR, Laboratoire MAST-SDOA,
F-77455 Marne La Vallée, Cedex 2, France
email: pierre.argoul@ifsttar.fr

Abstract

The transverse argumental vibration of a beam excited axially by an harmonic motion transmitted through intermittent or permanent elastic contact is studied. It is shown that this vibration is governed by a non-linear argumental equation, namely that a vibration in the fundamental transverse mode of the beam can occur when the frequency of the excitation is many times the frequency of the fundamental transverse mode. Two cases are considered : the hinged-(hinged-guided) case, and the clamped-(clamped-guided) case. A "natural" model is given. An approached smooth model is derived. The averaging method yields a standard system of differential equations for the smooth model. Numeric simulations allow a comparison between the natural model and the smooth model.

Keywords— non-linear; argumental oscillator; beam; axial excitation; transverse; spatial modulation; Van der Pol representation.

Contents

1 Introduction.

The so-called argumental oscillator has a stable motion consisting of a periodic motion at a frequency next to its natural frequency when submitted to an external force whose frequency is close to a multiple of said natural frequency. One condition for the phenomenon to arise is that the external force be dependent on the space coordinate of the oscillator. An oscillator exhibiting such characteristics has been described in 1938 [1]. The word "argumental" was forged in 1973 [12]. Further developments were carried out [9, 10], particularly the multiple resonance and the quantum effect. Argumental oscillations have also been observed and described in [8, 13]. They have also been studied in [3–5].
A typical second-order ordinary differential equation for a one-degree-of-freedom argumental oscillator is:

$$\ddot{x} + 2\beta\omega_0\dot{x} + \omega_0^2 x = g_1(x) + g_2(x)cos(\nu t) \tag{1}$$

where x is the space coordinate, β is the damping factor, ω_0 is the natural angular velocity of the oscillator, g_1 and g_2 are functions of x, and ν is the angular velocity of the excitation.
In this paper, a beam submitted to an axial harmonic excitation is studied. When near its resting rectilinear position, the beam "senses" the excitation, and when in a sufficiently bended position, it does not sense the excitation any more. This is realized by way of an intermittent contact. It will be shown that this system obeys an argumental equation. This configuration should allow to study the behaviour of a structure when two elements are in contact with each other, but can become disconnected, depending on their instantaneous transverse deformation. This situation can occur either by design or after damaging. In this paper, two models are studied, called "natural model" and "smooth model". A solution of the differential equations pertaining to the smooth model is carried out, using the averaging method. A comparison is made between numerical simulations on the natural model and the solution provided by the averaging method. In [6], these results are used to establish symbolic properties of the stationary regime. Experimental results are given in [7].

2 System configuration.

The schematic system configuration is as shown in Fig. 1. A beam is represented, with its left end S and right end M, in an clamped-(clamped-guided) configuration. Point M is intermittently pushed to the left by a plate C, which is linked to a point A via a spring. $\vec{F}$ is the force intermittently applied by plate C to the beam's right end in M. F is negative when the beam is in compression. Point A is in harmonic motion horizontally in the figure, in such a manner that the contact between plate C and point M be intermittent when the beam and point A are vibrating. When the beam is in resting (i.e. rectilinear) position and point A is in center position, the force applied to point M is denoted by F_0.

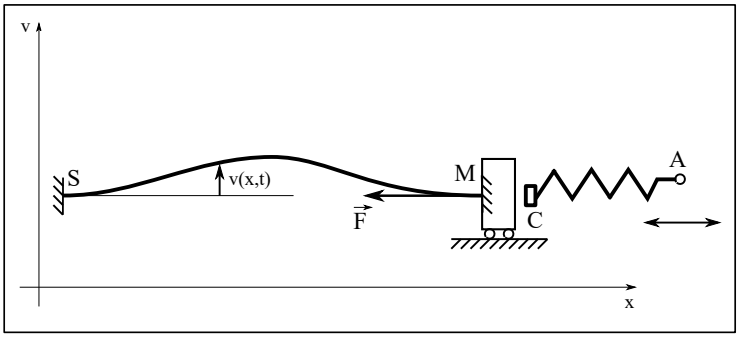

Figure 1: system configuration. x is the horizontal abscissa, v is the transverse displacement, t is the time, and $\vec{F}$ is the force applied by plate C to the beam at point M.

3 Modelling.

In this section, a first model will be studied, called "natural model", because it is deduced directly from simple physical laws and the arrangement of the components beam, spring, and points M and A. This leads to a discontinuous model, involving a C^0-class function for the external force, due to the intermittent nature of the contact at point M.
Then a second model will be studied, called a "smooth model", because it is an approximation to the natural model. This model is not as close to physical reality as the natural model, but, in exchange, involves a C^∞-class function for the external force, easier to manipulate.
Then a solution of the differential equations pertaining to the smooth model is carried out, using the averaging method. Finally, a comparison is made between numerical simulations on the natural model and the solution provided by the averaging method. Using the symbolic relations derived from the averaging method, properties of the stationary regime are given.

3.1 Expression of point M's abscissa x_M.

This expression will be needed to calculate the force F. As the beam bends, point M moves to the left. Define L = beam's length and x_M = point M's abscissa. On the beam, define the curvilinear abscissa from point S to current point (x, v) as $s(x, v, t)$. A classical method to calculate x_M is as follows.
As the beam is considered inextensible, point M's curvilinear abscissa is always equal to L, i.e.

$$s(x_M, v, t) = L = \int_0^{x_M} \sqrt{1 + \left(\frac{\partial v(u,t)}{\partial u}\right)^2}\, du \tag{2}$$

Then, using the limited development $\sqrt{1+\left(\frac{\partial v(u,t)}{\partial u}\right)^2} \approx 1+\frac{1}{2}\left(\frac{\partial v(u,t)}{\partial u}\right)^2$ inside Eq. (2), and considering that $\int_0^{x_M}\left(\frac{\partial v(u,t)}{\partial u}\right)^2 du \approx \int_0^{L}\left(\frac{\partial v(u,t)}{\partial u}\right)^2 du$, obtain:

$$x_M \approx L - \frac{1}{2}\int_0^{L}\left(\frac{\partial v(u,t)}{\partial u}\right)^2 du \tag{3}$$

Then, consider that the transverse motion is expressed as

$$v(x,t) = Lq_1(t)\varphi(x), \tag{4}$$

where $\varphi(x)$ is the modal form of the first mode and $q_1(t)$ is the amplitude as a function of time, both $\varphi(x)$ and $q_1(t)$ being adimensioned.

Hinged-(hinged-guided) case. In this case, consider that the first mode is

$$\varphi(x) = \sin\left(\pi\frac{x}{L}\right) \tag{5}$$

Clamped-(clamped-guided) case. In this case, consider that the modal form of the first mode is (see [Pecker, chap.8, p.169]):

$$\varphi(x) = B_1\left[\sin(ax) - 1.0178\cos(ax) - \sinh(ax) + 1.0178\cosh(ax)\right]$$

with B_1 arbitrary.
Approach this modal form with

$$\varphi(x) = \frac{1}{2}\left(1-\cos\left(\frac{2\pi x}{L}\right)\right), \tag{6}$$

It can be seen in Fig. 2 that, if $B_1 = 0.6024$, the approaching curve is close to the original curve.

Conclusion about both cases. Substituting expression (5) or (6) into Eq. (4), then $v(x,t)$ into (3), obtain:

$$x_M(t) \approx L\left(1-\frac{\pi^2}{4}q_1^2(t)\right)$$

for both the hinged-(hinged-guided) case and the clamped-(clamped-guided) case.

3.2 Natural model of force F.

Define x_A =point A's abscissa, $x_{A0} = \overline{x_A}$, where the overline notation means the averaging operation versus time. It can be seen from Fig. 1 that, provided there is contact between C and M, and denoting by F_0 the force F when $x_A = x_{A0}$:

$$F - F_0 = k(x_A - x_{A0} + L - x_M) \tag{7}$$

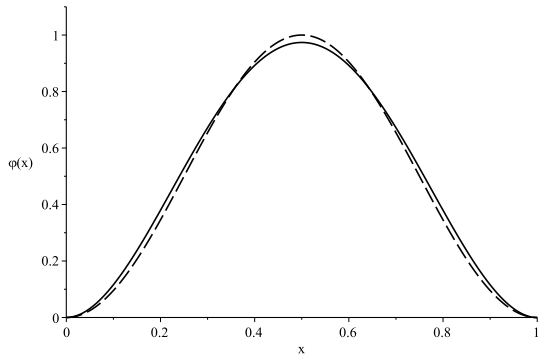

Figure 2: Approached modal form: exact (solid line), approached (dashed line).

where F is the expression of force, k is the spring's stiffness, and x_M is given by (7).
Define a_A as the amplitude of A's harmonic motion, normalized by L, i.e. $x_A(t) = x_{A0} + L\, a_A \cos(\nu t)$. Hence, Eq. (7) writes, taking into account (7):

$$F = F_0 + kL\left(a_A \cos(\nu t) + \frac{\pi^2}{4} q_1^2(t)\right) \tag{8}$$

If the contact is intermittent, i.e. if, from time to time, points M and A become sufficiently distant from each other to yield a positive value for the right-hand member of (8), it holds:

$$\begin{cases} F(q_1,t) = F_0 + kL\left(a_A \cos(\nu t) + \frac{\pi^2}{4} q_1^2(t)\right) & if\ F_0 + kL\left(a_A \cos(\nu t) + \frac{\pi^2}{4} q_1^2(t)\right) \leq 0 \\ F(q_1,t) = 0 \qquad\qquad otherwise \end{cases} \tag{9}$$

where F is denoted $F(q_1,t)$ because it depends on $q_1(t)$ and t. This constitutes the natural model of force F.

Upper bound for a_A. In this paper, the critical buckling force on the beam is considered never being reached nor exceeded. Therefore, it is necessary that $|F(q_1,t)| < F_B$ at all times, which, knowing that $|F(q_1,t)| \leq |F(0,t)|$ for any q_1 (and that the equality occurs), translates to $|F(0,t)| < F_B$ at all times, i.e. $-F_0 + kLa_A < F_B$. Finally, the upper bound of a_A can be expressed as:

$$a_A < \frac{F_B + F_0}{kL} \tag{10}$$

This value is referred to in this paper as the "Model validity upper limit".

Case of permanent contact. Putting $F < 0$ in Eq. (8), deduce that the condition for the contact to be permanent is: $a_A \cos(\nu t) + \frac{\pi^2}{4} q_1^2(t) < -F_0/(kL)$ at all times. The worst case is when $\cos(\nu t) = 1$, which leads to:

$$a_A < -\frac{F_0}{kL} - \frac{\pi^2}{4} q_1(t)^2 \tag{11}$$

This relation will be used hereinafter.

3.3 Smooth model of force F.

In this section, a truncated sinusoid is approximated by a sinusoid of same frequency and of lower amplitude, whose extremums are adjusted in reference to the truncated sinusoid. In addition, a truncated parabola is approximated by a smooth function. The combination of those two approximations leads to a continuous model.

High line and Low line. An approaching function F_{approx} for $F(x,t)$ will be defined below. Define, for the sake of clarity, y_{approx} and y_{exact} by $y_{approx}(x,t) = F_{approx}(x,t)/(kL)$ and $y_{exact}(x,t) = F(x,t)/(kL)$. Also, denote $q_1(t)$ by x.
The case where $F_0/(kL) < 0$ when $x = 0$ will be studied. That is, when the external excitation is off and the beam is at rest, there is contact between points M and C. In Figs. 3 to 6, various plots of the beam's transverse motion are represented. The values of the parameters are as follows: $F_0/(kL) = -2\ 10^{-3}$, $a_A = 1.8\ 10^{-3}$.
The case represented is when $\frac{F_0}{kL} + a_A < 0$, i.e. when the beam is at rest and the excitation is on, the contact between points M and C is never disrupted. This can be seen in Fig. 3.
The plot of y_{exact} is a sinusoid, which may be truncated or not, represented in the Figs. 3 to 6 by a solid line, along with the plot of y_{approx} in dashed line, and dotted construction lines showing the entirety of the truncated sinusoid, as well of various indications.
As soon as the sinusoid crosses the line $y = 0$, it gets truncated, and the only remaining part is located below said line.
From Eq. (9), it can be seen that the dotted horizontal marker line labelled $F_0/(kL) + a_A + \pi^2 x^2/4$ locates the top of the untruncated sinusoid, while the marker line labelled $F_0/(kL) - a_A + \pi^2 x^2/4$ locates the bottom of said sinusoid. The dotted horizontal markers labelled "High line" and "Low line" locate the highest (resp. lowest) point of the remaining part of the sinusoid after truncation.
Knowing that the excitation frequency is significantly greater than the beam's frequency (at least four times greater), consider that during one period of the excitation, the value of x is approximately constant, and the force F can be represented as a pure sinusoid, possibly truncated. It can be seen that the more x increases, the more the plot of y_{exact} (solid line) moves to the top of the figure,

and the less the remaining part of the sinusoid is significant.
Denoting by Hl and Ll the High line's and Low line's ordinates, it holds:

$$\begin{cases} Hl(x) = \dfrac{F_0}{kL} + a_A + \dfrac{\pi^2 x^2}{4} & if\ \dfrac{F_0}{kL} + a_A + \dfrac{\pi^2 x^2}{4} \leq 0 \\ Hl(x) = 0 & otherwise \end{cases}$$

and

$$\begin{cases} Ll(x) = \dfrac{F_0}{kL} - a_A + \dfrac{\pi^2 x^2}{4} & if\ \dfrac{F_0}{kL} - a_A + \dfrac{\pi^2 x^2}{4} \leq 0 \\ Ll(x) = 0 & otherwise \end{cases}$$

The method employed in this section consists in approximating the exact function y_{exact} by a full sinusoid y_{approx} located between the High line and the Low line. It holds:

$$y_{approx}(t) = \frac{High\,line + Low\,line}{2} + \frac{High\,line - Low\,line}{2}\cos(\nu t) \tag{12}$$

$$= Mean(y_{approx}) + Ampl(y_{approx})\cos(\nu t) \tag{13}$$

where $Mean(f)$ denotes the mean value of function f over one period of f and $Ampl(f)$ denotes the amplitude of function f, i.e. half the difference between the maximum and minimum values of $f(t)$ over one period of f.

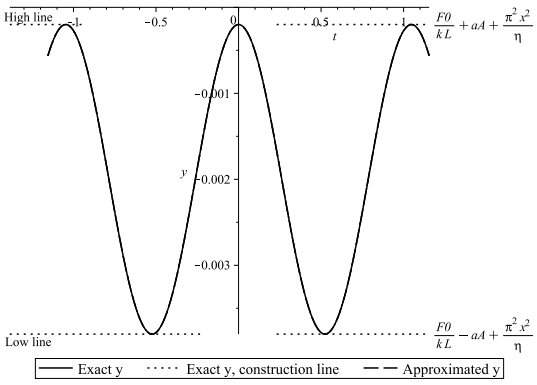

Figure 3: Exact and approached $y = F/(kL)$, with $x_{ref} = 0.0$, $a_A = -0.9\dfrac{F_0}{kL}$.

Approximation to a truncated parabola. An approximation to following class C^0-function J will be needed hereinafter. Define function $J(x)$ as follows:

$$\begin{cases} J(x) = \alpha + \beta x^2 & if\ \alpha + \beta x^2 \leq 0 \\ J(x) = 0 & otherwise \end{cases}$$

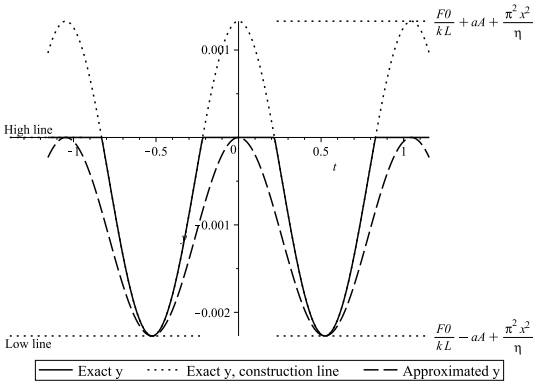

Figure 4: Exact and approached $y = F/(kL)$, with $x_{ref} = 0.015$, $a_A = -0.9\dfrac{F_0}{kL}$.

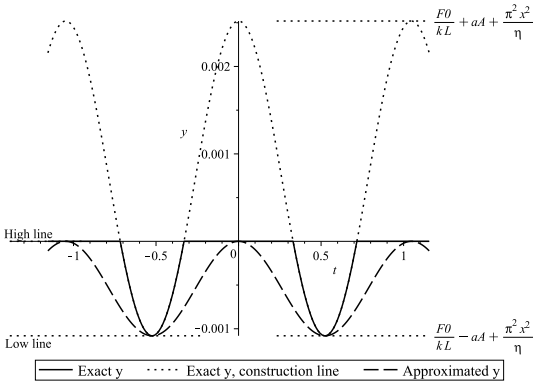

Figure 5: Exact and approached $y = F/(kL)$, with $x_{ref} = 0.02$, $a_A = -0.9\dfrac{F_0}{kL}$.

with $\alpha < 0$ and $\beta > 0$. This is a class C^0-function. Consider (see Fig. 7) that function

$$J_{approx} = \frac{\alpha}{1 + \lambda\frac{\beta}{\alpha}x^2} \tag{14}$$

with $-8 \leq \lambda \leq -2$, is a fair approximation to $J(x)$. J_{approx} is of class C^∞.

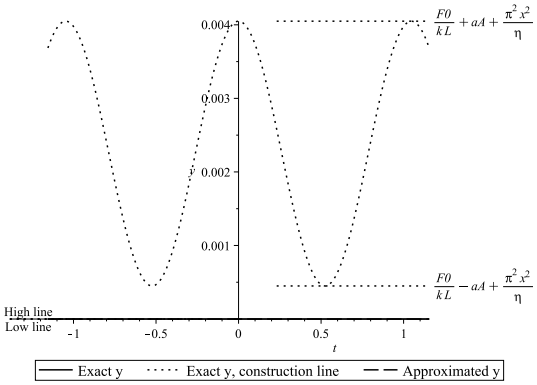

Figure 6: Exact and approached $y = F/(kL)$, with $x_{ref} = 0.025$, $a_A = -0.9\dfrac{F_0}{kL}$.

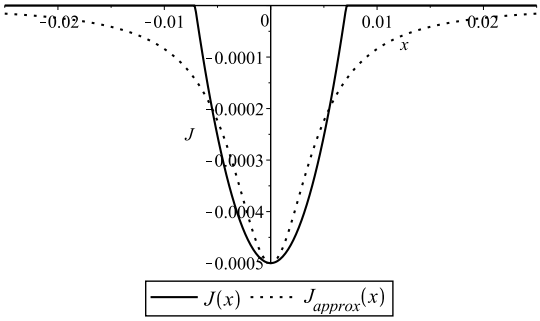

Figure 7: Exact and approached J, with $\dfrac{F_0}{kL} = -0.1\ 10^{-2}$, $a_A = 0.05\ 10^{-2}$.

Approximation to the amplitude of function y_{approx}. Define $a_{Acrit} = \left|\dfrac{F_0}{kL}\right| = -\dfrac{F_0}{kL}$, and form the expression of $Ampl(y_{approx}) = (Hl - Ll)/2$:

$$\begin{cases} Ampl(y_{approx}) & = a_A \qquad if\ \dfrac{\pi^2}{4}x^2 \leq a_{Acrit} - a_A \\ Ampl(y_{approx}) & = -\dfrac{1}{2}\left(\dfrac{F_0}{kL} - a_A + \dfrac{\pi^2}{4}x^2\right) \qquad if\ a_{Acrit} - a_A < \dfrac{\pi^2}{4}x^2 \leq a_{Acrit} + a_A \\ Ampl(y_{approx}) & = 0 \qquad if\ a_{Acrit} + a_A < \dfrac{\pi^2}{4}x^2 \end{cases}$$

which, using (14), can be approximated by:

- if $a_A < a_{Acrit}$:

$$Ampl(y_{approx}) \approx \frac{a_A}{1 + Bx^2} \tag{15}$$

- otherwise:

$$Ampl(y_{approx}) \approx \frac{1}{2} \frac{-\frac{F_0}{kL} + a_A}{1 + Bx^2} \tag{16}$$

with $B = -\dfrac{\pi^2 kL}{4F_0}$.

Approximation to the mean value of function y_{approx}. Form the expression of $Mean(y_{approx}) = (Hl + Ll)/2$:

$$\begin{cases} Mean(y_{approx}) & = \dfrac{F_0}{kL} + \dfrac{\pi^2}{4}x^2 \qquad if\ \dfrac{\pi^2}{4}x^2 \leq a_{Acrit} - a_A \\ Mean(y_{approx}) & = \dfrac{1}{2}\left(\dfrac{F_0}{kL} - a_A + \dfrac{\pi^2}{4}x^2\right) \qquad if\ a_{Acrit} - a_A < \dfrac{\pi^2}{4}x^2 \leq a_{Acrit} + a_A \\ Mean(y_{approx}) & = 0 \qquad if\ a_{Acrit} + a_A < \dfrac{\pi^2}{4}x^2 \end{cases}$$

which, using (14), can be approximated by:

- if $a_A < a_{Acrit}$:

$$Mean(y_{approx}) \approx \frac{F_0}{kL} \frac{1}{1 + Cx^2} \tag{17}$$

- otherwise:

$$Mean(y_{approx}) \approx \frac{1}{2} \frac{\frac{F_0}{kL} - a_A}{1 + Cx^2} \tag{18}$$

with $C = -\dfrac{\pi^2 kL}{2F_0}$.

Approximation to the F function. Substituting Equations (15), (16), (17) and (18) into Eq. (13), and substituting F_{approx} for kLy_{approx}, obtain:

- if $a_A < a_{Acrit}$:

$$F_{approx} = F_0 \left(1 - \frac{Cx^2}{1 + Cx^2}\right) + \frac{kLa_A}{1 + Bx^2} \cos(\nu t) \tag{19}$$

- otherwise:

$$F_{approx} = \frac{1}{2}(F_0 - kL\, a_A) \left(1 - \frac{Cx^2}{1 + Cx^2}\right) - \frac{1}{2} \frac{F_0 - kL\, a_A}{1 + Bx^2} \cos(\nu t) \tag{20}$$

with $x = q_1(t)$ =temporal adimensioned coordinate vs the first modal component of the beam, a_A =point A's adimensioned amplitude, F_0 =axial force applied to the beam when it is rectilinear and point A is in central position, k =spring's stifness, L =beam's length, and $C = 2B = -\dfrac{\pi^2 kL}{2F_0}$.

4 Second-order differential equation of motion.

Eq. (7) gives x_M as a function of q_1, while Equations (19) and (20) give an approximated expression of the external force as a function of x and t. Substituting these expressions into the general equation to the modal coordinates, it is possible to obtain a second-order ordinary differential equation in $x(t)$.

4.1 Classical transverse motion of an axially-excited beam.

The classical equation of motion of an axially-excited Euler-Bernoulli beam with nonrotating and planar motion and neglecting stretching is [11, Chap. 14]:

$$\frac{\partial^2}{\partial x^2}\left(EI(x)\frac{\partial^2 v}{\partial x^2}\right)+\frac{\partial}{\partial x}\left(S(x)\frac{\partial v}{\partial x}\right)+m(x)\frac{\partial^2 v}{\partial t^2}=p(x,t) \tag{21}$$

where $v(x,t)$ is the transverse displacement, E is the elastic modulus, $I(x)$ is the second moment of area of the beam's cross-section, $S(x)$ is the axial force, $m(x)$ is the mass per unit length, and $p(x,t)$ is a transverse distributed force. Consider herein that $p=\rho Sg$, where g =acceleration of gravity.
Next, consider that the axial force S depends only on the beam's actual deformation state q_1 (as defined in Section 3) and on time, which does not change the form of Equ. (21). Denote said force by $-F(q_1,t)$ (so that $F(q_1,t)<0$ in case of compression, to be consistent with convention of Section 3). Also, consider that the flexural rigidity $EI(x)$ and the transverse distributed force are constant over the beam. Moreover, consider that the mass per unit length is constant over the beam, and denote it by ρS, where ρ is the mass density and S is the beam's cross-section area. Finally, use the dot notation to denote differentiation with respect to time, and classically introduce a damping effect as $2\beta'\dot{v}$ to obtain

$$\rho S\ddot{v}+EI\frac{\partial^4 v}{\partial x^4}-F(q_1,t)\frac{\partial^2 v}{\partial x^2}+2\beta'\dot{v}=\rho Sg \tag{22}$$

Using a change of variables $v(x,t)=Lq(t)\varphi(x)$, obtain:

$$\rho S\ddot{q}(t)\varphi(x)+EI\varphi^{(4)}(x)q(t)-F(q_1,t)\varphi''(x)q(t)+2\beta'\varphi(x)\dot{q}(t)=\rho Sg \tag{23}$$

4.2 Projection onto the first mode.

Projecting Eq. (23) onto the first mode, obtain, for the hinged-(hinged-guided) case and modal form as per Equ. (2):

$$\ddot{q}_1(t)+\frac{2\beta'}{\rho S}\dot{q}_1(t)+\left(\frac{\pi}{L}\right)^4\frac{EI}{\rho S}q_1(t)+\left(\frac{\pi}{L}\right)^2\frac{1}{\rho S}F(q_1,t)q_1(t)-\frac{4g}{\pi L}=0 \tag{24}$$

with $v(x,t)=Lq_1(t)\sin\left(\frac{\pi}{L}x\right)$.
And for the clamped-(clamped-guided) case:

$$\ddot{q}_1(t)+\frac{2\beta'}{\rho S}\dot{q}_1(t)+\left(\frac{2\pi}{L}\right)^4\frac{EI}{3\rho S}q_1(t)+\left(\frac{\pi}{L}\right)^2\frac{1}{\rho S}F(q_1,t)q_1(t)-\frac{2g}{3L}=0 \tag{25}$$

with $v(x,t)$ as per (6).
Introduce the beam's critical buckling force

$$F_B = \frac{\pi^2 EI}{a_3^2 L^2} \tag{26}$$

where L is the beam's length and a_3 is a coefficient equal to 1 in the hinged-(hinged-guided) case and 1/2 in the clamped-(clamped-guided) case.
Equations (24) and (25) can be rewritten into a unique expression:

$$\ddot{q}_1(t) + \frac{2\beta'}{\rho S}\dot{q}_1(t) + a_1\left(\frac{\pi}{L}\right)^2 \frac{F_B}{\rho S} q_1(t) + a_1\left(\frac{\pi}{L}\right)^2 \frac{1}{\rho S} F(q_1,t) q_1(t) - a_2 \frac{g}{L} = 0 \tag{27}$$

with $a_1 = 1$, $a_2 = 4/\pi$ and $a_3 = 1$ in the hinged-(hinged-guided) case, and $a_1 = 4/3$, $a_2 = 2/3$ and $a_3 = 1/2$ in the clamped-(clamped-guided) case.

4.3 Equation of motion with the natural model.

By implementing the natural model of the external force, this second-order differential equation will be of use below, to assess the quality of the smooth approximated model which is given in section 3.
Transforming Eq. (27) while denoting $q_1(t)$ by y for the sake of clarity, obtain:

$$\ddot{y} + 2\beta\omega_0\dot{y} + \omega_0^2 y = -\omega_0^2 \frac{y}{F_B/(kL) + C_2/(kL)} F(y,t) + a_2 \frac{g}{L}$$

with $\omega_0^2 = a_1\left(\frac{\pi}{L}\right)^2 \frac{F_B + C_2}{\rho S}$, $\beta\omega_0 = \frac{\beta'}{\rho S}$, and C_2 =arbitrary constant.
Then, choosing $C_2 = F_0$ to have ω_0 consistent with its natural value when $F \equiv 0$, obtain:

$$\ddot{y} + 2\beta\omega_0\dot{y} + \omega_0^2 y = -\omega_0^2 \frac{y}{F_B/(kL) + F_0/(kL)} F(y,t) + a_2 \frac{g}{L} \tag{28}$$

with $\omega_0^2 = a_1\left(\frac{\pi}{L}\right)^2 \frac{F_B + C_2}{\rho S}$ and

$$\begin{cases} F(y,t) = F_0 + kL\left(a_A\cos(\nu t) + \dfrac{\pi^2}{4}y^2(t)\right) & \text{if } F_0 + kL\left(a_A\cos(\nu t) + \dfrac{\pi^2}{4}y^2(t)\right) \le 0 \\ F(y,t) = 0 & \text{otherwise} \end{cases} \tag{29}$$

4.4 Equation of motion with the smooth model.

By implementing the smooth model of the external force, this second-order differential equation will allow to use the averaging method, and then to derive symbolic relations. Recall that $a_{Acrit} = \left|\frac{F_0}{kL}\right| = -\frac{F_0}{kL}$. Because the expression of force F in Eq. (27) differs depending on the sign of $a_A - a_{Acrit}$, two cases

must be distinguished here, depending on the sign of $a_A - a_{Acrit}$. Denoting y for $q_1(t)$, obtain, substituting F_{approx} as given in Equations (19) and (20) into Eq. (27):

- If $a_A < a_{Acrit}$:

$$\ddot{y} + 2\beta\omega_0\dot{y} + \omega_0^2 y = -\omega_1^2 \frac{Cy^3}{1+Cy^2} + a_2\frac{g}{L} + \omega_1^2 \frac{a_A}{\frac{F_0}{kL}} \frac{y}{1+By^2}\cos(\nu t)$$

- If $a_A \geq a_{Acrit}$:

$$\ddot{y} + 2\beta\omega_0\dot{y} + \omega_0^2 y = -\omega_2^2 \frac{Cy^3}{1+Cy^2} + a_2\frac{g}{L} - \omega_2^2 \frac{y}{1+By^2}\cos(\nu t) \tag{30}$$

with

$$\omega_0^2 = a_1\left(\frac{\pi}{L}\right)^2 \frac{F_B + F_0}{\rho S},\ \omega_1^2 = -\frac{F_0}{F_B + F_0}\omega_0^2,$$
$$\omega_2^2 = -\frac{F_0 - a_A kL}{2F_B + F_0 - a_A kL}\omega_0^2,\ C = 2B = -\frac{\pi^2 kL}{2F_0}. \tag{31}$$

Those equations are argumental equations similar to Eq. (1).

5 Applying the averaging method.

The averaging method [2] is applied to the second-order differential equation of motion in y with the approximated (smooth) form of the external force.

5.1 Reduced time.

Introducing the reduced time τ, classically defined as $\tau = \omega_0 t$, and using from now on the dot notation to denote differentiation with respect to τ, obtain

$$\ddot{z} + 2\beta\dot{z} + z = g_1(z) + g_2(z)cos\left(\frac{\nu}{\omega_0}\tau\right) \tag{32}$$

with $z(\tau) \equiv y(t)$ and

- If $a_A < a_{Acrit}$:
  $g_1(z) = -\omega_1^2 \frac{Cz^3}{1+Cz^2} + a_2\frac{g}{L}$ and $g_2(z) = -\omega_{11}^2 \frac{z}{1+Bz^2}$
  with $\omega_1^2 = -\frac{F_0}{F_B + F_0}\ \omega_0^2$ and $\omega_{11}^2 = \frac{a_A kL}{F_B + F_0}\omega_0^2$.
- If $a_A \geq a_{Acrit}$:
  $g_1(z) = -\omega_2^2 \frac{Cz^3}{1+Cz^2} + a_2\frac{g}{L}$ and $g_2(z) = -\omega_2^2 \frac{z}{1+Bz^2}$
  with $\omega_2^2 = -\frac{F_0 - a_A kL}{2F_B + F_0 - a_A kL}\omega_0^2$.

It should be noted that ω_{11} and ω_2 depend on the excitation's amplitude a_A, and that it is assumed that $|F_0 - a_A kL| < 2F_B$. Then, to use the classical averaging method's results [2, 10] recalled in [3], in which the second-order reduced-time differential equation in z writes

$$\ddot{z} + z = -2\beta\dot{z} - g(z) + AH(z)E(\tau), \tag{33}$$

identify (32) with (33), obtaining

$$\begin{cases} g(z) = -\dfrac{g_1(z)}{\omega_0^2} \\ AH(z) = \dfrac{g_2(z)}{\omega_0^2} \\ E(\tau) = \cos\left(\dfrac{\nu}{\omega_0}\tau\right) \end{cases}$$

with $H(z) = -\dfrac{z}{1+Bz^2}$ and

$$\begin{cases} A(a_A) = \dfrac{kLa_A}{F_B + F_0} & \text{if } \ a_A < a_{Acrit} \\ A(a_A) = -\dfrac{F_0 - a_A kL}{2F_B + F_0 - a_A kL} & \text{otherwise} \end{cases} \tag{34}$$

The choice of an expression for $H(z)$ which is the same in both cases allows to carry out only one calculus when it comes to Fourier decomposition below. And because A depends on a_A, it will be denoted from now on as $A(a_A)$.

5.2 Standard system.

Searching for a solution $z(\tau)$ close to a slowly-varying sinusoid, carry out the classical averaging method, beginning by a change of variables as follows:

$$\begin{cases} z(\tau) &= a(\tau)\sin(\rho\tau + \varphi(\tau)) \\ \dot{z}(\tau) &= a(\tau)\rho\cos(\rho\tau + \varphi(\tau)) \end{cases}$$

and obtain the standard system involving variables a and φ, which is the system which will be averaged:

$$\begin{cases} \dot{a} &= \dfrac{\cos(\theta)}{\rho}\left(-2\beta\rho a\cos(\theta) - g(a\sin(\theta)) + A(a_A)H(a\sin(\theta))E(\tau) + a\sin(\theta)(\rho^2 - 1)\right) \\ \dot{\varphi} &= -\dfrac{\sin(\theta)}{\rho a}\left(-2\beta\rho a\cos(\theta) - g(a\sin(\theta)) + A(a_A)H(a\sin(\theta))E(\tau) + a\sin(\theta)(\rho^2 - 1)\right) \end{cases}$$

with $\theta = \rho\tau + \varphi$, $\rho = \dfrac{\omega}{\omega_0}$, ω= constant to be determined (close to ω_0), $A(a_A)$ according to (34) and $E(\tau) = \cos\left(\dfrac{\nu}{\omega_0}\tau\right)$.

The reciprocal relations are as follows, knowing that $a(\tau)$ is always positive:

$$\begin{cases} a(\tau) & = \sqrt{z^2(\tau) + \left(\dfrac{\dot{z}(\tau)}{\rho}\right)^2} \\ \varphi(\tau) & = \arctan\left(\rho \dfrac{z(\tau)}{\dot{z}(\tau)}\right) - \rho\tau \ [2\pi] \end{cases} \tag{35}$$

These relations are of use to interpret the results of a solution to the second-order equation of the natural or smooth model in terms of Van der Pol representation, to compare them to the solution given by the averaged smooth model, which is natively in Van der Pol coordinates.

5.3 Averaged system.

Averaged expression relative to function G. Putting $G(a, a_A) = \overline{\sin(\theta) g(a\sin(\theta))}$, where the overline notation denotes averaging with respect to time over one period of the solution, and neglecting gravity, obtain:

- If $a_A < a_{Acrit}$:

$$G(a, a_A) = -\frac{1}{2} \frac{F_0}{F_B + F_0} a \left(1 - \frac{2}{Ca^2} + \frac{1}{Ca^2} \frac{2}{\sqrt{1 + Ca^2}}\right) \tag{36}$$

- If $a_A \geq a_{Acrit}$:

$$G(a, a_A) = -\frac{1}{2} \frac{F_0 - a_A kL}{2F_B + F_0 - a_A kL} a \left(1 - \frac{2}{Ca^2} + \frac{1}{Ca^2} \frac{2}{\sqrt{1 + Ca^2}}\right) \tag{37}$$

Decomposing function $H(a\sin(\theta))$ into a Fourier series of variable θ. This decomposition will allow an averaging of $H(a\sin(\theta))$ hereinafter.
$H(a\sin(\theta))$ being an odd function of variable θ, and being of period π, define its Fourier series coefficients h_q by

$$H(a\sin(\theta)) = \sum_{q=1,\ q\ odd}^{+\infty} h_q \sin(q\theta)$$

Then a calculus yields:

- If $a_A < a_{Acrit}$:
  $h_q = -a_A kL \dfrac{2}{B^{\frac{q+1}{2}}} \dfrac{(\sqrt{1 + Ba^2} - 1)^q}{\sqrt{1 + Ba^2} a^q}$

- If $a_A \geq a_{Acrit}$:
  $h_q = \dfrac{F_0 - a_A kL}{2} \dfrac{2}{B^{\frac{q+1}{2}}} \dfrac{(\sqrt{1 + Ba^2} - 1)^q}{\sqrt{1 + Ba^2} a^q}$

Calculus of $\overline{H(a\sin(\theta))}E(\tau)\cos(\theta)$. If $\dfrac{\nu}{\rho\omega_0}$ is an even integer (denoted by n), obtain $\overline{H(a\sin(\theta))E(\tau)\cos(\theta)} = \dfrac{1}{4}S_n\sin(n\varphi)$, with $S_n = h_{n-1} + h_{n+1}$.
Otherwise, $\overline{H(a\sin(\theta))E(\tau)\cos(\theta)} = 0$.

Calculus of $\overline{H(a\sin(\theta))}E(\tau)\sin(\theta)$. If $\dfrac{\nu}{\rho\omega_0}$ is an even integer (denoted by n), obtain $\overline{H(a\sin(\theta))E(\tau)\sin(\theta)} = -\dfrac{1}{4}D_n\cos(n\varphi)$, with $D_n = h_{n-1} - h_{n+1}$.
Otherwise, $\overline{H(a\sin(\theta))E(\tau)\sin(\theta)} = 0$.

Symbolic expressions of functions S_n and D_n . A calculus gives

$$S_n = -\frac{4}{a^{n+1}}\frac{(\sqrt{1+Ba^2}-1)^n}{B^{\frac{n}{2}+1}} \tag{38}$$

$$D_n = \frac{S_n}{\sqrt{1+Ba^2}} \tag{39}$$

Also:

$$\begin{aligned}\frac{1}{S_n}\frac{\partial S_n}{\partial a} &= \frac{1}{a}\left(\frac{n}{\sqrt{1+Ba^2}} - 1\right)\\ \frac{1}{D_n}\frac{\partial D_n}{\partial a} &= \frac{1}{a}\left(\frac{n}{\sqrt{1+Ba^2}} - 2 + \frac{1}{1+Ba^2}\right).\end{aligned} \tag{40}$$

ω_{00} and ρ_{00}. Recall that $\omega_0^2 = a_1\left(\dfrac{\pi}{L}\right)\dfrac{F_B+F_0}{\rho S}$. Put $\omega_{00} = \omega_0|_{F_0=0}$. It follows that ω_{00} is a constant parameter of the physical system. Then, introducing parameter ρ_{00}, and recalling that $\rho = \dfrac{\nu}{n\omega_0}$:

$$\begin{cases}\omega_0 = \omega_{00}\sqrt{\dfrac{F_B+F_0}{F_B}}\\ \rho = \rho_{00}\sqrt{\dfrac{F_B}{F_B+F_0}}\\ \rho_{00} = \dfrac{\nu}{n\omega_{00}}\end{cases} \tag{41}$$

It can be seen that ρ_{00} is also a constant parameter of the physical system. Because $F_0 \leq 0$, it holds $\rho \geq \rho_{00}$.
Also, define $\lambda = |F_0|/F_B = -F_0/F_B$.

Averaged standard system. The classical averaging calculus yields, if $n = \dfrac{\nu}{\rho\omega_0}$ is an even integer:

$$\begin{cases} \dot{a} &= \dfrac{A(a_A)}{4\rho} S_n(a)\sin(n\varphi) - \beta a \\ \dot{\varphi} &= \dfrac{G(a,a_A)}{\rho a} + \dfrac{A(a_A)}{4\rho a} D_n(a)\cos(n\varphi) - \dfrac{\rho^2-1}{2\rho} \end{cases} \tag{42}$$

with $A(a_A)$ defined as per Equ. (34), C by Equ. (31) and G per Equs. (36) and (37).
If $n = \dfrac{\nu}{\rho\omega_0}$ is not an even integer, it holds:

$$\begin{cases} \dot{a} &= -\beta a \\ \dot{\varphi} &= \dfrac{G(a,a_A)}{\rho a} - \dfrac{\rho^2-1}{2\rho} \end{cases}$$

that is, the motion equations are the same as if the system were disconnected from the excitation source.

6 Stationary condition.

Setting $\dot{a} = 0$ and $\dot{\varphi} = 0$ in system (42) constitutes the equations of the stationary condition:

$$\begin{cases} 0 &= \dfrac{A(a_A)}{4\rho} S_n(a_S)\sin(n\varphi_S) - \beta a_S \\ 0 &= G_1(a_S,a_A) + \dfrac{A(a_A)}{4a_S} D_n(a_S)\cos(n\varphi_S) - \dfrac{\rho^2-1}{2} \end{cases} \tag{43}$$

where a_S is the motion's amplitude and φ_S is the phase shift of said motion with respect to the excitation force, and function G_1 is defined as

$$G_1(a_S,a_A) = G(a_S,a_A)/a_S \tag{44}$$

β-curve, G-curve and stationary-solutions curve. Writing that $\sin^2(n\varphi_S) + \cos^2(n\varphi_S) = 1$, obtain from Equs. (43):

$$(4\rho\beta)^2 + 4\frac{S_n^2(a_S)}{D_n^2(a_S)}\left(2G_1(a_S,a_A) - (\rho^2-1)\right)^2 = \frac{A(a_A)^2 S_n^2(a_S)}{a_S^2} \tag{45}$$

This can then be written:

$$F_\beta(a_S) + 4\frac{S_n^2(a_S)}{D_n^2(a_S)} F_G^2(a_S) = 0 \tag{46}$$

with

$$F_\beta(a_S) = (4\rho\beta)^2 - \left(\frac{A(a_A)S_n(a_S)}{a_S}\right)^2,$$

and

$$F_G(a_S, a_A) = 2G_1(a_S, a_A) - (\rho^2 - 1)$$

Define the "β-curve" as the curve representing the solution to equation $F_\beta(a_S) = 0$. Also, define the "G-curve" as the curve representing the solution to equation $F_G(a_S, a_A) = 0$. Finally, define the "Stationary-solutions curve" as the curve whose each point represents one stationary solution to Eq. (45).

Excitation threshold. It is of interest to be able to assess the minimum value of a_A versus a_S along a stationary-solutions curve, because this value of a_A is the excitation threshold allowing the argumental phenomenon with given parameters n, β, F_B, F_0, L, k, f_{00} and ρ_{00}. The numerical plots show that the minimum of a_A seems to be close to an intersection point of the β-curve and the G-curve. Therefore, it is natural to carry out a local study around said intersection point to confirm this impression. Said local study, along with other symbolic calculus, is carried out in [6].

Graphic representation of the stationary solutions in the (a_S, a_A)-plane. Fig. 8 shows the implicit stationary-solutions curve, obtained numerically, giving a_A against a_S for the values of parameters given in the figure's legend. The solid-line curve represents the solutions to Eq. (45), with a minimum at point A_{min}. Observation of Fig. 8 shows that, due to the distinction pertaining to the position of a_A against a_{Acrit}, the solutions to System (43) can be seen as a set composed of two parts, depending on the position of the current stationary-solution's representative point with respect to the horizontal line $a_A = a_{Acrit} = |F_0|/(kL)$, herein called the "critical line":

- An upper part (above said line) composed of two arcs, in contact at their higher extremities at one point, and at their lower extremities at said line.
- A lower part, constituted by a V-shaped curve, presenting a minimum at point A_{min}.

The upper and lower parts are connected at the critical line. The right (resp. left) arc and the right (resp. left) part of the V-shaped curve represent the stable (resp. unstable) stationary solutions. For a given value of the excitation, i.e. a given amplitude a_A, there are two possible values for a_S, represented by points S and U. Point S is the stable stationary condition, while point U is the unstable one. The V-shaped curve represents cases where there is permanent contact between the beam under test (BUT) and the excitation source when the BUT is in rectilinear position. In these cases, the contact may or may not remain permanent when the BUT enters a transversal vibration, depending on the spring's stiffness and the amplitudes of transversal vibration of the BUT and of the excitation source.
Fig. 9 shows the layout of the curves for another set of parameters. In this case, the intersection between the G-curve and the β-curve never exists under the critical line, and therefore, the V-shaped part of the stationary-solutions curve never shows up.

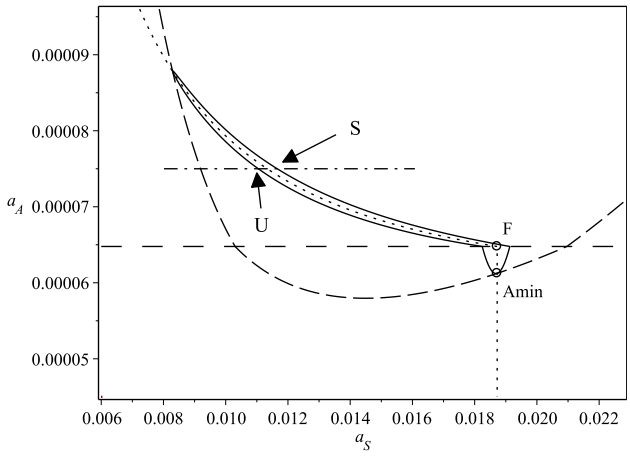

Figure 8: An example of stationary conditions for the averaged system with the smooth model of the external force. a_S is the stationary-motion's amplitude, a_A is the excitation's amplitude. The dash-dotted line shows the value of a_A which will be used for the Van der Pol representation of Fig. 10. The dotted line is the G-curve. The solid line is the set of stationary solutions to the averaged smooth model. The dashed line is the β-curve. S and U respectively represent the stable and unstable stationary conditions. They are located at the intersection of the stationary-solutions curve and the dash-dotted line. The space-dashed horizontal line is the "critical line". A_{min} is at the minimum of the stationary-solutions curve. Parameter values are: $n = 6$, $\beta = 2.4\ 10^{-3}$, $F_B = 51N$, $F_0 = -8N$, $L = 0.95m$, $k = 130\ kN/m$, $f_{00} = 6.615Hz$, $f_{shaker} = 39.500711Hz$, $\rho_{00} = 0.9952308$, $\lambda = 0.1569$. Model validity upper limit=$3.48\ 10^{-4}$.

7 Smooth model of the external force.

In this section, the symbolic expressions found above will be tested and illustrated. The approximated smoothed form of the external force is studied using the numerical solutions to the averaged system (42). By the way, a comparison between the numerical solutions to the averaged system (42) and the solutions to the original second-order equation (30) will test the validity of the averaging method.

7.1 Smooth model of the external force and averaging method.

Figure 8 shows a plot of the numerical solutions to System (43), giving the stationary solutions to System (42). The parameters are those of a typical experimental setup. Each point of the plot represents a stationary motion, i.e. a motion with constant amplitude and constant phase. The abscissae are the system's motion amplitude, while the ordinates are the excitation's, i.e. the

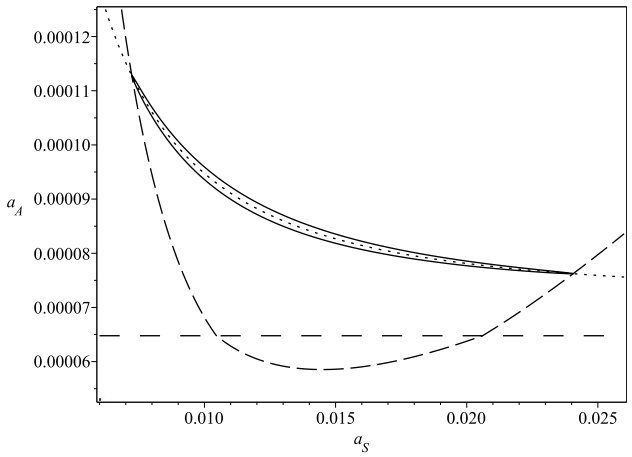

Figure 9: Stationary conditions in the case $\rho_{00} > 1$ for the averaged system with the smooth model of the external force. The graphical-element descriptions and parameter values are the same as for Fig. 8, except $f_{shaker} = 39.88845Hz$ and $\rho_{00} = 1.005$.

motion amplitude of Point A represented in Fig. 1. An example of Van der Pol plot representing the solutions to the averaged system (42) with the smooth model is given in Fig. 10 for $n = 6$. When an attractor center or a saddle point is identifiable, it is one of the points of a stationary-solutions curve in the (a_S, a_A)-plane.

7.2 Smooth model of the external force and original second-order equation.

An example of Van der Pol plot representing solutions to the original second-order equation (30) with the smooth model is given in Fig. 11, to be compared to Fig. 10. It can be seen that the curves are very close to each other.

7.3 Conclusion.

The comparison between the results of the original second-order equation and those of the averaged system shows that there is almost no difference between them. Therefore from now on, consider that the comparison between the smooth model and the natural model will be carried out by comparing the results of the averaged system for the smooth model and the results of the original second-order equation for the natural model.
Having carried out the calculus about the smooth model, it remains to be done the calculus about the natural model.

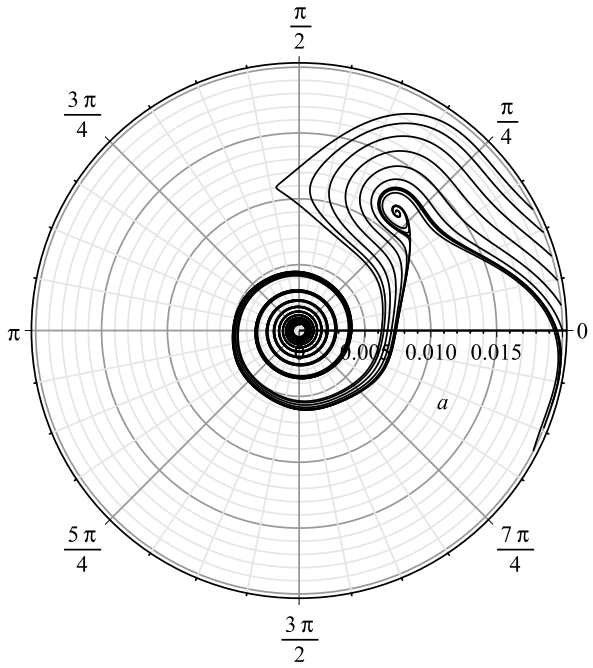

Figure 10: Van der Pol plot, averaged system with the smooth model of the external force. a is the motion's amplitude, φ is the motion's phase. The value of a_A which is used is $7.5\ 10^{-5}$. The initial values are 0.02 for a and -0.475 for φ. The parameter values are the same as in Fig. 8.

8 Natural model of the external force.

In this section, the natural model of the external force is studied with numerical solution of the original second-order equation (28). The solutions to the original second-order equation with the natural model (28), i.e. with the natural form of the external force as given by Eq. (9), are obtained by the Runge-Kutta solver, giving y as a function of t. To construct the corresponding Van der Pol plots, first convert the solution into reduced-time, and then use the reciprocal relations (35), with $\rho = \nu/(\omega_0 n)$ to obtain $a(\tau)$ and $\varphi(\tau)$. Finally, apply a lowpass filter on $a(\tau)$ and $\varphi(\tau)$ to partially cancel out the oscillations of the curves about the mean trajectory. An example of Van der Pol plot obtained by this method is given in Fig. 12, to be compared with Figs. 10 and 11. Here the comparison shows that the curves are similar, but not identical. This is not surprising, because the smooth model is built upon approximations. Particularly, with the help of Fig. 22, it can be seen that between the two models, offsets can be expected on the stationary amplitude a_S and on the stationary phase φ_S. In the Van der Pol plots, these offsets are offsets are in the positions of the

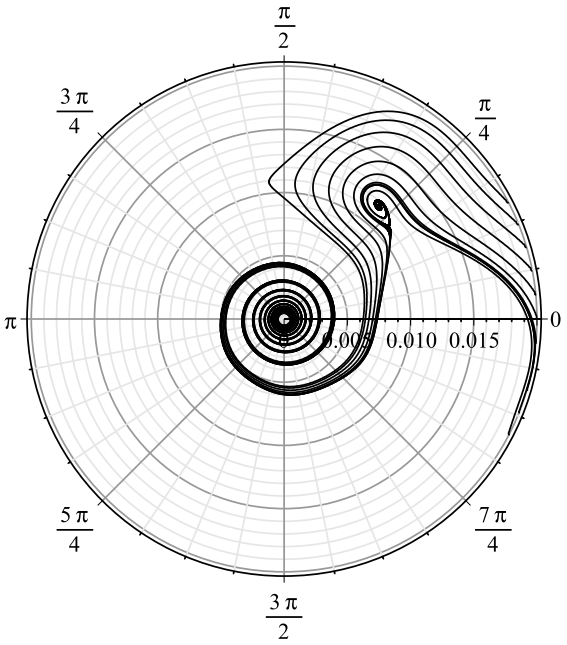

Figure 11: Van der Pol plot, original second-order equation with the smooth model of the external force. a is the motion's amplitude, φ is the motion's phase. The parameter values and initial values are the same as in Fig. 8.

attractors' centers and of the saddle points. In the (a_S, a_A))-plane, the offsets are directly identifiable as two distinct points, one on a stationary-solutions curve, the other as a discrete point resulting from a numerical calculus and a manual identification on a Van der Pol plot.

Construction of the stable and unstable stationary-regime representative points. In the averaged smooth model, those two points are calculated for a given excitation a_A. In the natural model, they are determined graphically by observation of the Van der Pol plots. The points representing a stable stationary condition are the centers of spirals, while those corresponding to an unstable condition are the saddle type. For instance, in Fig. 12, the stable S point is at radius 0.0115 and angle 5 $\pi/16$, while the unstable U point is locatable at the peak of the curve near the point at radius 0.008 and angle $\pi/2 + 0.6\pi/16$, and then, knowing the problem's invariance through a rotation of $2\pi/n$, duplicated 6 times around the circle of radius 0.008, yielding a point U' at $\pi/2 + 0.6\pi/16 - 2\pi/6 \approx 3.26\pi/16$.

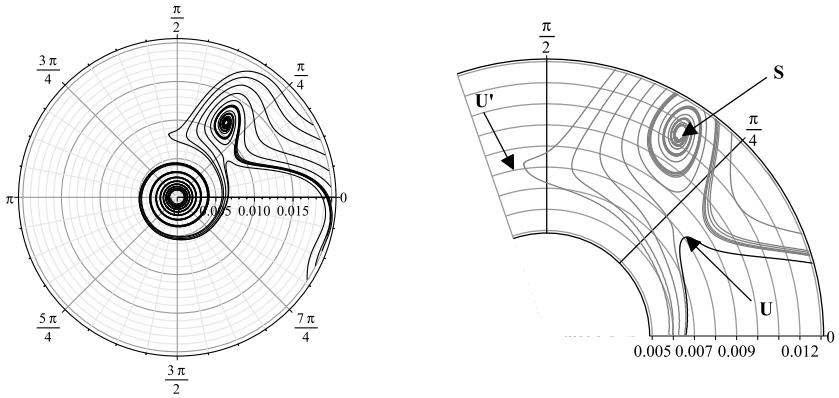

(a) (b)

Figure 12: Van der Pol plot, original second-order equation with the natural model of the external force. (a): global view; (b): detailed view. The radius is the motion's amplitude, the angle is the motion's phase. The parameter values are the same as in Fig. 8, except $a_A = 6.5\ 10^{-5}$ and initial value of $\varphi = -0.565$.

9 Other considerations.

9.1 A case where $n = 14$.

To illustrate that the argumental phenomenon can arise for values of n greater than 4 or 6, a plot of the averaged-system's stationary-solutions for the smooth model with $n = 14$ is showed in Figs. 13 and 14.

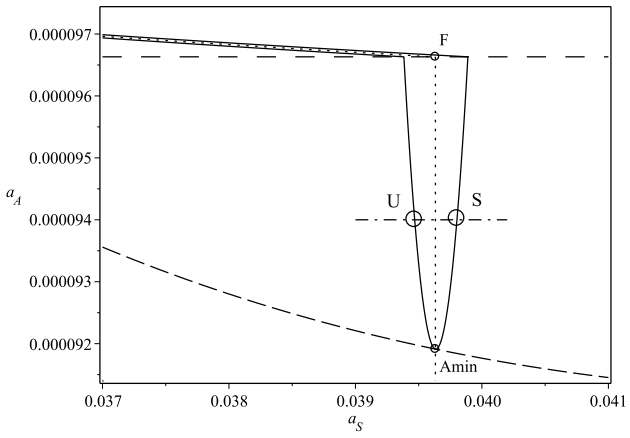

Figure 13: Stationary condition, averaged system with the smooth model of the external force. a_S is the stationary-motion's amplitude, a_A is the excitation's amplitude. S and U are the stable and unstable stationary solutions to the averaged system when $a_A = 0.094\ 10^{-3}$. Parameter values are: $n = 14$, $\beta = 1.6\ 10^{-3}$, $F_B = 51\ N$, $F_0 = -22.95\ N$, $L = 0.95\ m$, $k = 250\ kN/m$, $f_{00} = 6.615\ Hz$, $f_{shaker} = 92.14695\ Hz$, $\rho_{00} = 0.995$, Model validity upper limit (in ordinate aA)$=1.18\ 10^{-4}$.

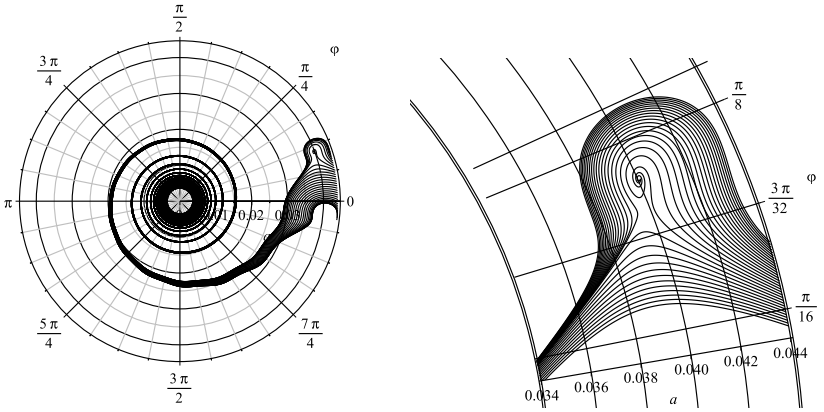

(a) (b)

Figure 14: Van der Pol representation for Fig. 13 when $a_A = 0.094\ 10^{-3}$. (a): main view, (b): zoomed view, with more trajectories to bring out the stationary points.

9.2 Case of permanent contact.

In this paragraph, it will be shown that, in certain cases, the argumental phenomenon can exist while the contact between the excitation source and the BUT remains permanent. From Eq. (11), deduce that, in the (a_S, a_A)-plane, the equation defining the region where the contact is permanent is:

$$a_A < -\frac{F_0}{kL} - \frac{\pi^2}{4}a_S^2 = a_{Acrit} - \frac{\pi^2}{4}a_S^2 \tag{47}$$

This is an arc of parabola with vertex at $(a_S = 0, a_A = a_{Acrit})$, and intersecting the abscissae axis at $a_S = \frac{2}{\pi}\sqrt{a_{Acrit}}$. Two examples of argumental phenomenon for a BUT with permanent contact are given, in the (a_S, a_A)-plane, in Figs. 15 and 18. Fig. 16 is a Van der Pol representation, in rectangular coordinates, of the motion yielded by the smooth model with the parameters of Fig. 15 and $a_A = 5.0\,10^{-5}$ (a_A about half below the Model validity upper limit). A number of threads can be seen, each thread corresponding to given initial conditions. Fig. 17 is the same, but with the natural model. For clarity's sake, there are less threads represented in Fig. 17 than in Fig. 16; it can be seen that each thread is shaky (although some filtering has been applied to enhance readability); this is because the natural model is based on the second-order initial equation of motion, whose solution renders every detailed motion due to the external force's action. The smooth model, after application of the averaging method, cancels out all tiny vibrations around the slowly-varying sinusoid which is the solution to the averaged system of equations (42), and it follows that the threads in the Van der Pol representation for this model are smooth. Comparison of Figs. 16 and 17 shows that the attractors' centers are localized in the neighbourhood of each other.

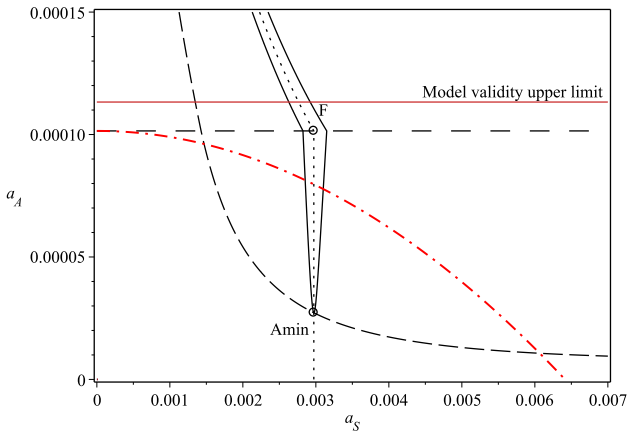

Figure 15: A case of permanent contact with $n = 4$. The dash-dotted line is the border of the region where the contact is permanent. Parameters: $n = 4$, $F_B = 51N$, $F_0 = -24.1N$, $\lambda = 0.472549$, $\rho_{00} = 0.8$, $\beta = 0.0024$, $k = 2.5\ 10^5$, $f_{shaker} = 21.168Hz$, $f_{00} = 6.615Hz$, $L = 0.95m$, Model validity upper limit=$1.1326\ 10^{-4}$. Only the part of the stationary-solutions curve (solid line) located below this limit is relevant.

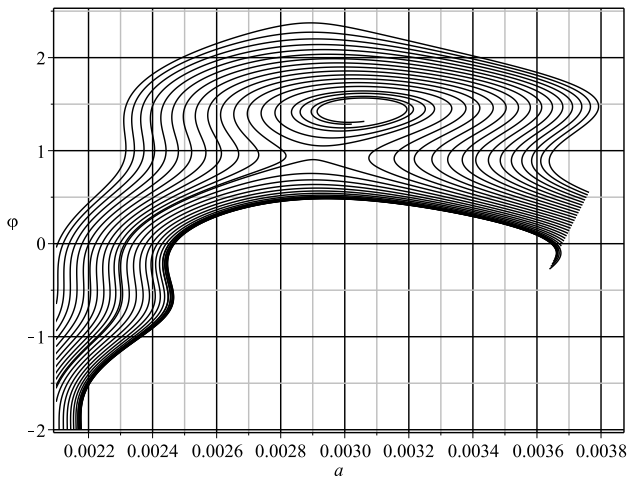

Figure 16: Smooth-model Van der Pol simulation in rectangular coordinates. Parameters are those of Fig. 15, plus $a_A = 5\ 10^{-5}$.

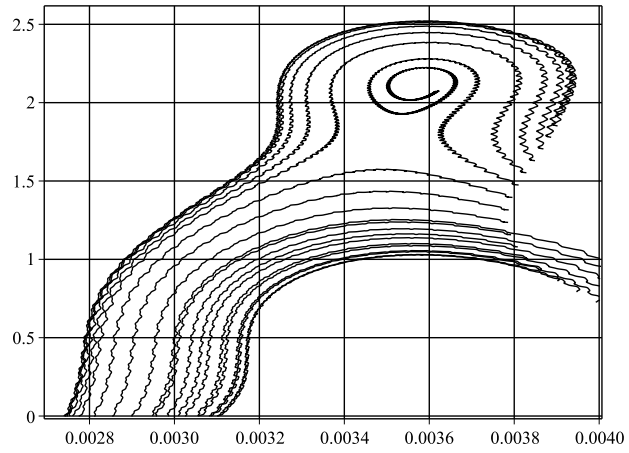

Figure 17: Natural-model Van der Pol simulation in rectangular coordinates. Parameters are those of Fig. 16.

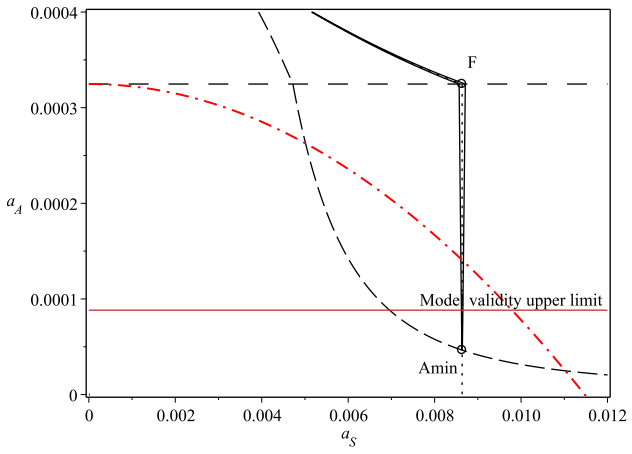

Figure 18: A case of permanent contact with $n = 6$. The dash-dotted line is the border of the region where the contact is permanent. Parameters: $n = 6$, $F_B = 51N$, $\lambda = 0.7862745$, $\rho_{00} = 0.75$, $\beta = 0.0008$, Model validity upper limit=8.8 10^{-5}. Only the part of the stationary-solutions curve (solid line) located below this limit is relevant.

10 Model comparison.

In this section, using the results from sections above, a comparison between the exact and the approximated forms of the external force will test the validity of the smooth model versus the natural model.

10.1 Case $n = 4$.

Figs. 19 and 20 show a comparison between averaged system (with smooth model) and second-order equation (with natural model) for $n = 4$. It can be seen that, for this set of parameters, the smooth model gives results very close to those of the natural model for low values of the excitation's amplitude a_A. In the natural model, the "V" part of the curve is skewed, while it is not in the smooth model. This is because of an approximation made in the smooth model, namely in the expression of B. A model using the expression $B = -\frac{\pi^2}{2}\frac{1}{\frac{F_0}{kL} - a_A}$ yields this skewed layout of the "V" part of the stationary-solutions curve. However, for simplification purposes, and to allow analytical expression to be brought out, it has been decided to rather use the expression $B = -\frac{\pi^2}{4}\frac{kL}{F_0}$. It can be seen that for high values of a_A, the smooth model gives solutions which do not exist in the natural model. However, in the lower region, there is a good agreement between smooth and natural models.
Fig. 21 gives a few stationary-solutions curves, with parameters of Fig. 19, for various values of F_0.

10.2 Case $n = 6$.

For $n = 6$, Fig. 22 uses the same parameters as Fig. 8, except $F_0 = -7.2N$, to plot the stationary solutions to the smooth model with addition of points representing the stationary results of the natural-model simulations. The full range of values for parameter a_A yielding a stationary condition in the natural model have been explored for the parameters mentioned in Fig. 8. Here the value of F_0 is close to the lower limit where the argumental phenomenon disappears. It can be seen that in this case, the results of the smooth model are not as close to the natural model as in Fig. 19, but still give a good assessment.
Figure 22 shows that the parameter ranges for the argumental oscillations to arise turn out to be quite narrow. Hence the knowledge of the symbolic formulas of the smooth model constitute a guide to the choice of parameters for the natural model, which is closer to physical reality. The comparison of the curves in Figs. 10 and 11 shows that the averaging method, for the parameters used, yields very good results. The curves in Fig. 12 are fairly close to those in Figs 10 and 11. This must be viewed in the global context of Fig. 22, where it can be seen that the parameter windows for the argumental phenomenon to

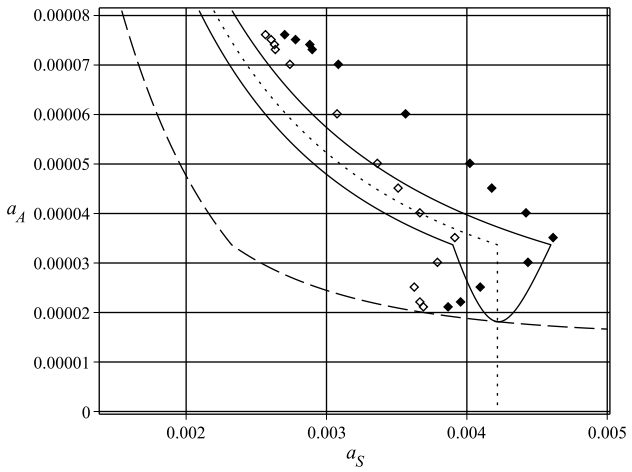

Figure 19: Stationary condition, a_A (point A's amplitude) against a_S (stationary motion's amplitude). Comparison between second-order equation (with natural model), represented as diamonds, and averaged system (with smooth model), represented as a solid line. The G-curve is the dotted line, while the β-curve is the dashed line. Parameters are: $n = 4$, $F_B = 51N$, $F_0 = -6.4N$, $f_{00} = 6.615Hz$, $\beta = 2.4\ 10^{-3}$, $L = 0.95m$, $k = 200\ 10^3 N/m$, $f_{shaker} = 25.849813$, $\rho_{00} = 0.976939$, $\lambda = 0.12549$. In the same way as in Fig. 8, where stable and unstable stationary solutions are represented as an infinity of points belonging to solid lines, a discrete series of stable (solid diamonds) and unstable (diamonds) stationary points are represented here. Model validity upper limit=$2.347\ 10^{-4}$.

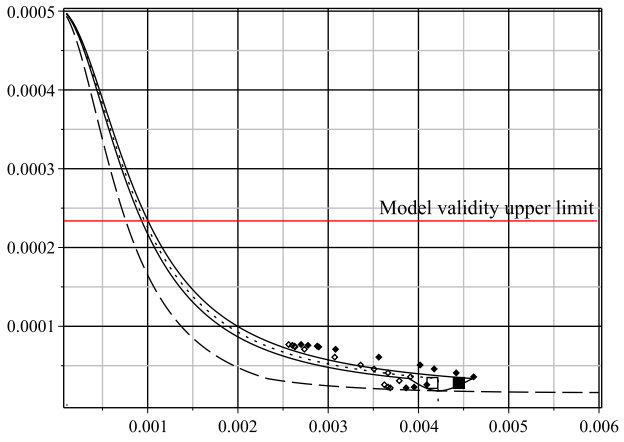

Figure 20: This view shows the whole picture containing Fig. 19.

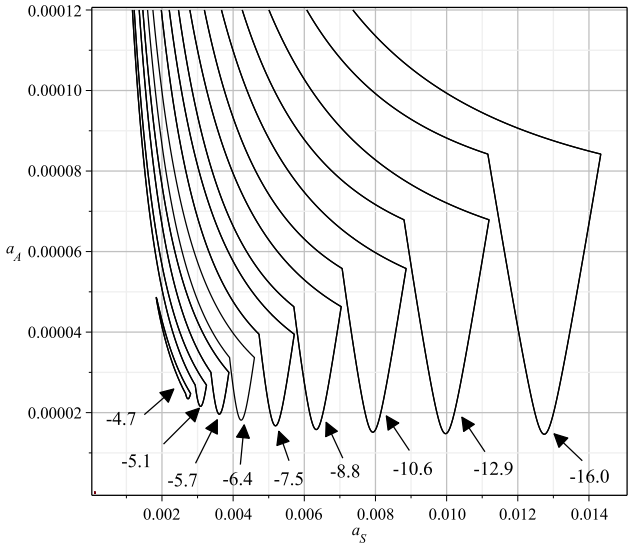

Figure 21: Stationary condition, a_A (point A's amplitude) against a_S (stationary motion's amplitude). A few stationary-solutions curves for the smooth model, for various values of F_0, denoted by arrows in the graph. Parameter values are the same as in Fig. 19. Worst-case (i.e. for $F_0 = -16.0$) Model validity upper limit=1.84 10^{-4}.

arise are narrow with respect to the possible parameter ranges.

10.3 Discussion.

The necessity that the contact be located in a narrow parameter window explains why argumental phenomenons arise rarely in the context of structure vibration. Said windows are even narrower as n increases. The example used in Figs. 8 to 12 is for $n = 6$, but Figs. 13 and 14, to be compared with Fig. 8, show how the situation evolves when $n = 14$. In this case, the windows for a_A and a_S are respectively about 30% and 3% of the central values of a_A and a_S, against 45% and 70% for $n = 6$; the ratio F_0/F_B is 78% against 10%.
It can be seen in the Van der Pol plots that if the right amplitude excitation (a_A) is applied and the beam is given an initial amplitude (preferably larger than the expected stationary amplitude a_S), the system's trajectory will either end up into an attractor or decrease to zero due to damping, depending on initial conditions. A study of the capture probability by the attractor (the spiral) is given in [5].
Fig. 22 shows that the parameter ranges for the argumental oscillations to arise turn out to be quite narrow. Hence the knowledge of the symbolic formulas of

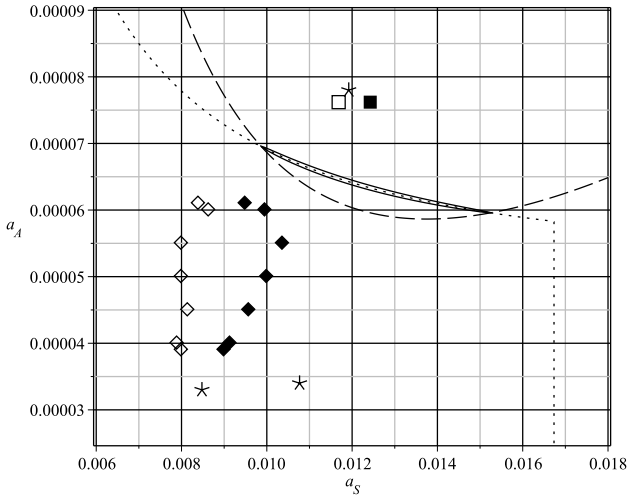

Figure 22: Stationary condition, a_A (point A's amplitude) against a_S (stationary motion's amplitude). Comparison between second-order equation (with natural model) and averaged system (with smooth model). Parameters are the same as in Fig. 8, except $F_0 = -7.2N$. In the same way as in Fig. 8, stable and unstable stationary points are represented. Results of numerical simulations using the natural model are represented as diamonds (unstable points) and solid diamonds (stable points). Model validity upper limit=3.54 10^{-4}.

the smooth model constitute a guide to the choice of parameters for the natural model, which is closer to physical reality.
Figure 23 gives some stationary-solutions curves with same parameters as Fig. 22, except for F_0, which takes a set of values.
The coordinates of points representing the constant-amplitude motion, stable and unstable stationary condition, show that, given the high sensitivity of the Van der Pol representation and the zoom window used, the results of the smooth-model simulation are indeed a good guide to those of the natural model. They allow to numerically explore the natural model with more efficiency.

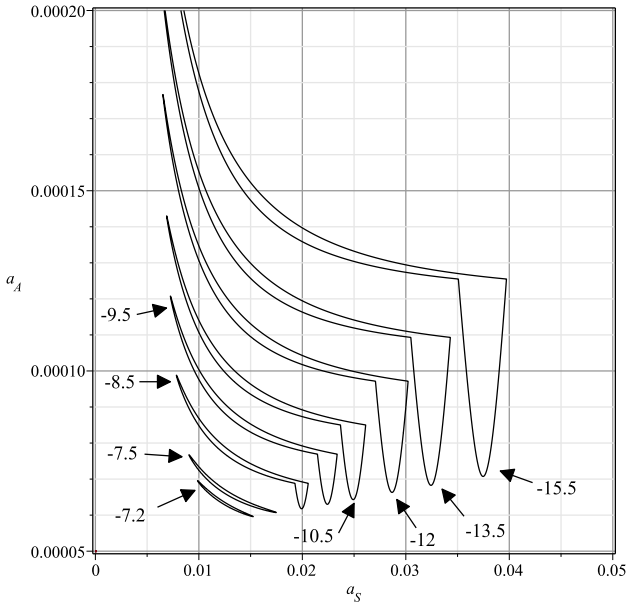

Figure 23: Stationary condition, a_A (point A's amplitude) against a_S (stationary motion's amplitude). A few stationary-solutions curves for the smooth model, for various values of F_0, denoted by arrows in the graph. Parameter values are the same as in Fig. 22. Worst-case (i.e. for $F_0 = -15.5$) Model validity upper limit=$2.87\ 10^{-4}$.

11 Conclusion.

It has been shown that when a beam under test is submitted, through a permanent or an intermittent elastic contact, to an harmonic axial excitation which is a multiple of twice the beam's fundamental transverse frequency, it can enter a stationary regime, where its transverse vibration has a frequency which is the beam's fundamental transverse frequency. Besides the classical resonant case, where the axial excitation is twice the fundamental frequency of the beam, this constitutes an argumental phenomenon.
This situation can be encountered when two beams are placed head-to-head, in axial contact, permanent or intermittent. It could seem intuitive that the argumental phenomenon is due to the intermittent contact. It can be seen that the phenomenon can also arise when the contact is permanent. Therefore, to avoid the argumental phenomenon, it is not sufficient to arrange the system so as to maintain a permanent contact.

References

[1] M.J. Béthenod. Sur l'entretien du mouvement d'un pendule au moyen d'un courant alternatif de fréquence élevée par rapport à sa fréquence propre. *Comptes rendus hebdomadaires de l'Académie des sciences*, 207(19):847–849, November 1938. (in French).

[2] N. Bogolioubov and I. Mitropolski. *Les méthodes asymptotiques en théorie des oscillations non linaires*. Gauthiers-Villars, 1962.

[3] D. Cintra and P. Argoul. Non-linear argumental oscillators: Stability criterion and approximate implicit analytic solution. *Journal to be determined*, 2016. (submitted).

[4] D. Cintra and P. Argoul. Nonlinear argumental oscillators: A few examples of modulation via spatial position. *Journal of Vibration and Control*, 2016. (online publication, pre-printing).

[5] D. Cintra and P. Argoul. Attractor's capture probability in nonlinear argumental oscillators. *Communications in Nonlinear Science and Numerical Simulation*, 48:150 – 169, 2017.

[6] D. Cintra, G. Cumunel, and P. Argoul. Transverse argumental vibration of a beam excited axially by an harmonic motion transmitted through permanent or intermittent elastic contact: a few properties in symbolic form. *Journal to be determined*, 2017. (submitted).

[7] D. Cintra, G. Cumunel, and P. Argoul. Transverse vibration of a beam excited axially by an harmonic motion transmitted through intermittent elastic contact: experimental results. *Journal to be determined*, 2017. (submitted).

[8] B. Cretin and D. Vernier. Quantized amplitudes in a nonlinear resonant electrical circuit. In *2009 Joint Meeting of the European Frequency and Time Forum and the IEEE International Frequency Control Symposium, vols 1 and 2*, volume 1 & 2, pages 797–800, Besançon, France, April 2009. Joint Meeting of the 23rd European Frequency and Time Forum/IEEE International Frequency Control Symposium.

[9] D. Doubochinski. *Argumental oscillations. Macroscopic quantum effects.* SciTech Library, August 2015.

[10] D.B. Doubochinski and J.B. Doubochinski. Amorçage argumentaire d'oscillations entretenues avec une série discrète d'amplitudes stables. *E.D.F. Bulletin de la direction des études et recherches, série C mathématiques, informatique*, 3:11–20, 1991. (in French).

[11] J.L. Humar. *Dynamics of Structures*. A.A. Balkema, 2001.

[12] D. I. Penner, D. B. Doubochinski, M. I. Kozakov, A. S. Vermel, and Yu. V. Galkin. Asynchronous excitation of undamped oscillations. *Soviet Physics Uspekhi*, 16(1):158–160, July-August 1973.

[13] J.P. Treilhou, J. Coutelier, J.J. Thocaven, and C. Jacquez. Payload motions detected by balloon-borne fluxgate-type magnetometers. *Advances in Space Research*, 26(9):1423–1426, 2000.